Examining Chemical Composition of Gas Turbine-Emitted Organic Aerosol using Positive Matrix Factorization (PMF)

Liam D. Smith[1*], James Allan[1,2], Hugh Coe[1], Ernesto Reyes-Villegas[1], Mark P. Johnson[3], Andrew Crayford[4], Eliot Durand[4] & Paul I. Williams[1,2]

[1]*School of Natural Sciences, University of Manchester, Manchester, UK*

[2]*National Centre for Atmospheric Science, UK*

[3]*Rolls-Royce plc, Derby, UK*

[4]*Department of Engineering, Cardiff University, Cardiff, UK*

[*]*Corresponding author. Tel: N/A; Fax: N/A;*

Email: liam.smith-2@manchester.ac.uk

Postal address: Simon Building, Brunswick St, Manchester M13 9PS

Abstract

In this paper, the characteristics of non-refractory aerosol using an International Civil Aviation Organization (ICAO) compliant sampling system emitted from two gas turbine relevant sources are reported, namely: an in-service turboshaft helicopter engine and a development combustor rig. Positive Matrix Factorisation (PMF) analysis was applied on an Aerosol Mass Spectrometer's (AMS) Unit Mass Resolution (UMR) organic aerosol (OA) data to identify three chemical factors: one unburnt fuel factor (AlkOA; Alkane Organic Aerosol) and two factors formed through oxidative processes: Semi Volatile Oxygenated Organic Aerosol (SV-OOA) and Quenched Organic Aerosol (QOA). The AlkOA factor's mass concentration correlated with Elemental Carbon (EC), an incomplete combustion tracer. The SV-OOA factor's mass concentration correlated with AMS-detected sulphate and Organic Carbon (OC) as characterised by a Sunset semi-continuous Analyser, with a high proportion of the OC converted to CO_2 at lower temperatures (≤475 °C) during the OC analysis, suggesting a higher volatility. The QOA factor's mass concentration corresponded with higher quantities of OC converted to CO_2 at the highest temperature (870 °C) during the OCEC analysis protocol. The QOA factor comprised large quantities of AMS-detected organic mass concentrations (20-50%) for the IP Rig. In addition, issues were seen with the OCEC analyser, and future strategies for operation for sampling from aviation sources are considered. The work characterises the available chemical speciation present in the particulate matter phase within an ICAO compliant nvPM sampling system for in-service and development combustor rigs, and comparisons are made between mass spectra seen within this methodology and in evolved plumes.

Keywords: aircraft; emissions; organic; volatile; aerosol; lubrication; oil; PMF

1. Introduction

Particulate Matter (PM) has well established links with disease and premature death (van Berlo, Hullman & Schins, 2012), with links to the PM's composition being an important factor for its health impacts (Valavanidis, Fiotakis & Vlachogianni, 2008). In areas with aviation hubs, gas turbine-emitted particulate matter (PM) has been observed to degrade air quality over distances of up to 18 kilometres downwind (Yim et al, 2013; Hudda et al, 2014; Hudda & Fruin, 2016; Hudda et al, 2016). Research has found links between airport emissions and premature death (Yim et al, 2013), and more specifically, between gas turbine generated PM exposure and toxicity in human bronchial cells (He et al, 2018; Jonsdottir et al, 2019). While the findings are preliminary, there is some indication that the composition of airport-originated PM changes the level of toxicity in these cells (He et al, 2018) and that particle mass measurements alone do not explain the range of effects witnessed (Jonsdottir et al, 2019). These findings suggest the importance of greater compositional understanding of aircraft PM. Gas turbine generated PM is characterised into two categories: non-volatile particulate matter (nvPM) and volatile particulate matter (vPM). nvPM is a term defined for standardised measurements of gas turbine engine emissions, for PM which is solid at engine exit plane and does not volatilize at temperatures up to 350 °C (ICAO, 2017; SAE, 2018). vPM formed in an aircraft's plume is unregulated and lacks a standardised definition in the ICAO standards. However, it has been described in the scientific literature as gas turbine PM which forms downstream of the combustor exit and does not exist in the PM phase at temperatures greater than 350 °C (Petzold et al, 2011). The vPM is comprised of sulphate and organic matter. It has been estimated that 53% of $PM_{2.5}$

emitted at airports consisted of OC and SO_4 (Stettler et al, 2011). Sulphuric compounds evolve from the fuel's sulphur (Lukachko et al, 2008) while organic PM comes from combustion products or the engine's lubrication oil (Yu et al, 2010; Yu et al, 2012). The presence of lubrication oil in the sample is dependent on where the engine vents (core or below the engine), the integrity of the seals, the mixing of the plume and the subsequent positioning of the sampling probe. Considering the contributions by vPM, alongside that post exhaust treatment is not possible in the case of gas turbine engines, there is a growing requirement for greater understanding in vPM composition and its measurement.

Emissions standards for nvPM have been developed by the International Civil Aviation Organisation's Committee on Aviation Environmental Protection (ICAO-CAEP) with the use of a largely standardised and well-defined sampling setup, which has been used in several studies (Crayford et al., 2013; Lobo et al, 2015; Lobo et al, 2016; Kiliç et al, 2018**;** Lobo et al, 2020). The ICAO system is designed to prevent coagulation of PM and provide consistent particle losses system to system. The system has not been designed to prevent formation of vPM, and some studies have successfully used the nvPM systems to collect organic vPM data (Lobo et al, 2015; Kiliç et al, 2018). In the studies, vPM organic mass concentrations taken from Aerosol Mass Spectrometers (AMS) were reported as either total mass or emission indices (EI) without further characterisation. Other research has conducted deeper analysis of the organic matrices of vPM (Timko et al, 2010; Timko et al, 2014; Yu et al, 2019) via in-situ on-wing emission measurements. Results from these methodologies are invaluable, however such experimental setups are likely incompatible with future engine certification and

introduce replicability issues due to extraneous variables (e.g. local wind conditions, background concentrations & restrictive nature of airport operations). Because of this, a repeatable testing methodology, like the existing ICAO nvPM system, could serve as an ideal scientific methodology and is more likely to be utilised for any possible future vPM emission standards. To the authors knowledge, to-date, no reported studies have conducted a deeper characterisation of the aerosol organic matrix measured using an ICAO compliant nvPM regulatory sampling system. Such a characterisation is necessary to provide indication as to whether the chemical information available in an ICAO compliant setup is likely to be consistent with evolved plume measurements. Such indication could help inform the development of future standards inclusive of vPM emissions. Using this insight for future readjustments of an existing system would save significant resources and effort in both standards testing and scientific research.

This paper provides a characterisation of organic vPM speciation using the ICAO compliant European Union Aviation Safety Agency (EASA) aircraft engine nvPM reference system. AMS and semi-continuous Organic Carbon and Elemental Carbon (OCEC) measurements were employed to assess the range of measurable chemical speciation available with this sampling methodology. Data were then analysed with the Multilinear Engine (ME-2; Canonaco et al, 2013; to examine oil contribution) & Positive Matrix Factorisation (PMF; Paatero & Tapper, 1994; Patero, 1999; Paatero & Tapper, 2009; for the remainder of the organic matrix) to analyse AMS vPM organic aerosol measurements taken from a Rolls-Royce Gnome Turboshaft helicopter engine (kerosene combustion and oil source) and an Intermediate Pressure (IP) combustor rig (Oil free source, kerosene combustion only) at near-exit plane distances to ensure vPM

formation.

2. Methodology

2.1 Setup

Tests were conducted - on the two aforementioned emission sources - at the Rolls-Royce Derby site from 28th November to 8th December 2017. The first source assessed was a Rolls-Royce Gnome Turboshaft helicopter engine, as used in prior aerosol studies where a description of the engine is reported (Olfert et al, 2017). The second source was Rolls-Royce's Intermediate Pressure (IP) combustor rig, developed as a tool for gas turbine fuel spray nozzle hardware ranking. Due to intellectual property rights, disclosure of further information regarding the fuel injector design used in this study is not permissible, however, the concept by which the development of the rig was based, is available in Makida et al. (2006). Both sources were fueled with JetA1 fuel, provided via the Rolls-Royce Derby on-site distribution network. While no fuel analysis was performed, the fuel employed at Rolls-Royce generally possesses an aromatic content between 17%-19% and sulphur content between 300-500ppm.

A non-scaled schematic of the experimental setup used in this study is available in Figure 1, which details the geometry, temperature and flow rates employed. The set-ups used on each combustion source were kept nominally identical, to afford consistency in vPM formation/composition. Details of the ICAO compliant EASA aircraft engine nvPM reference system (EASA, 2012) and University of Manchester instrument suite are detailed below. This sampling methodology has been characterized

for size dependent particle losses, with more information available in the ICAO literature (ICAO, 2017).

Exhaust samples from the Rolls-Royce Gnome Turboshaft helicopter engine were obtained using a single point probe (7.75mm ID) sampling from the engine's exhaust. Samples from the IP combustor rig were acquired using a water cooled (160 °C) multi-orifice piccolo sampling probe located downstream of the quenched flame. Undiluted samples were transported through insulated temperature controlled (160 °C) 7.75mm ID stainless steel sampling lines, ~2m in length for the Gnome engine and 4m for the IP combustor rig. These near-exit distances were chosen for practicality and may have facilitated limited vPM formation prior to dilution. The sample was then diluted with 60 ºC HEPA filtered air at an 8:1 dilution ratio using a Dekati DI-1000. It is noted that the dilution ratio was held nominally constant across all conditions tested, hence the mass and number concentrations presented have not been corrected for dilution. A heated 25-meter-long anti-static Polytetrafluoroethylene (PTFE) (Winkler-WAKG) sampling line was used to transport the sample outside the test cells to the suite of aerosol instruments at constant flow rates and temperatures of 25 slpm and 60 ºC respectively. Any excess flow from the dilutor was vented out of a spill port enabling constant sample flow and residence time after the dilution stage. A 60 ºC heated oven split the sample to the EASA nvPM number and mass concentration measurement analysers consisting of an AVL Particle Counter (APC), an Artium Laser Induced Incandescence soot instrument (LII 300, referred to in this publication as LII) and an AVL Micro Soot Sensor (MSS). APC and MSS results were not used in this analysis. It is noted that in the case of the LII - used to report EC mass concentration in this study

- refractory black carbon (rBC) is measured, however as per ICAO standards a thermo-optical gravimetric EC calibration constant (derived on a gas turbine engine) is applied to the measured LII signal, therefore converting these results from rBC to EC, and are listed as EC mass concentrations here. A Cambustion DMS 500 fast particle size measurement was made in parallel with the University of Manchester equipment using a flow splitter sampling from the EASA system's additional research sampling port. Care was taken to limit particle sampling bias; this was achieved by either ensuring equal flow splitting or where necessary using flow splitters with differing internal diameters to nominally match velocities.

The vPM was measured by the University of Manchester equipment. An Aerodyne Compact Time-of-Flight Aerosol Mass Spectrometer (C-ToF-AMS) characterized the chemical composition of the non-refractory PM. This is subsequently referred to as the AMS for brevity. Onasch et al. (2009), Yu et al. (2010) & Timko et al. (2014) have given descriptions of the usage of an AMS to measure aircraft exhaust PM. One notable limitation is that the AMS has a reduced transmission efficiency with vacuum aerodynamic diameters below 50nm (Liu et al, 2007) and it must be noted that this affects the results presented. Sulphate appears frequently in nucleation mode diameters (<20nm) within aircraft exhaust (Anderson et al, 1998; Onasch et al, 2009) and any statement of sulphate mass concentration will almost certainly be under-represented here as a result. The results in this paper focus on the composition of the organic mass concentration found in the 'soot mode', as defined by Yu et al. (2019). This mode ranges between 50nm – 100nm where the AMS has a high transmission efficiency (Liu et al, 2007). Particle Time-of-Flight (PToF) size distributions within the AMS are discussed

in the results. These particle size distributions are measured by particle time-of-flight, measured with starting time measured by the opening of the rotating beam chopper and the arrival time measured by the detection of chemicals by the mass spectrometer, more details on PToF analysis are presented by Yu et al (2019). The AMS was calibrated with an ammonium nitrate solution.

Complementary measurements to the AMS were taken simultaneously using a TSI 3776 Condensation Particle Counter (CPC) to measure total particle number concentrations (d50 = 2.5nm, upper size limit 2-3 μm), a TSI 3080 classifier Scanning Mobility Particle Scanner (SMPS) with a TSI 3085 nano DMA, to provide size distributions (measuring PM in the range of 8 – 150nm), and a Sunset Labs Semi-Continuous Organic Carbon Elemental Carbon (OCEC) Analyser for OC and EC mass concentrations. The OCEC was calibrated with a potassium phthalate solution. AMS PToF size distributions were taken for every condition presented in Figure 6 and are available in the supplementary material (S: Figure 1).

The OCEC analyzer is 'semi-continuous' in its operation; it takes in a sample for a designated time, depositing aerosol onto a quartz filter, for a user-defined sampling time, closes its inlet and then the deposited aerosol is thermal-optically analyzed using a user-selected temperature setting for analysis. The OCEC switches between drawing sample and analyzing the filter. All other instrument data presented is when the OCEC was sampling, unless otherwise stated. Further details of the OCEC Analyser's method are presented in section 2.4.

It is acknowledged that the use of any sampling system - inclusive of that used in this

study - results in particle losses, therefore PM mass concentrations shown in this paper are under-represented compared with those that entered the sampling probe inlet. However, it is noted that most of the PM mass is held in the larger sized particles, which are not significantly impacted by size dependent diffusional loss. As this paper is primarily intended to understand the source's proportional contributions to the OA mass concentration, and their associated trends, it is not anticipated that the uncertainty associated with system loss will affect the conclusions made. Where particle number concentrations and size distributions are utilized in the data analysis, they are intended for analyses of trends only, hence have not been corrected for loss. Alongside this, the applied setup is designed for engine certification purposes, and not for replication of particle processes which take place in-situ: in airports or at altitude. For example, the ICAO nvPM system was designed such so that dilution was applied as early as possible to prevent particle coagulation (Lobo et al, 2015), while the 60 ºC sampling line temperatures situated throughout the sampling system offer replicability regardless of ambient temperature. With this considered, some aspects of the design may alter some physical processes which would take place in an aircraft plume on a runway, for example: the two meters of insulated line combined with dilution afterward could prevent nucleation of particles or condensation of certain chemical compounds, which would have undergone such processes had it not been applied. Comparisons with in-situ (ranging from 10 to 50 meters) plume evolution measurements - taken in the existing literature - are made within this manuscript.

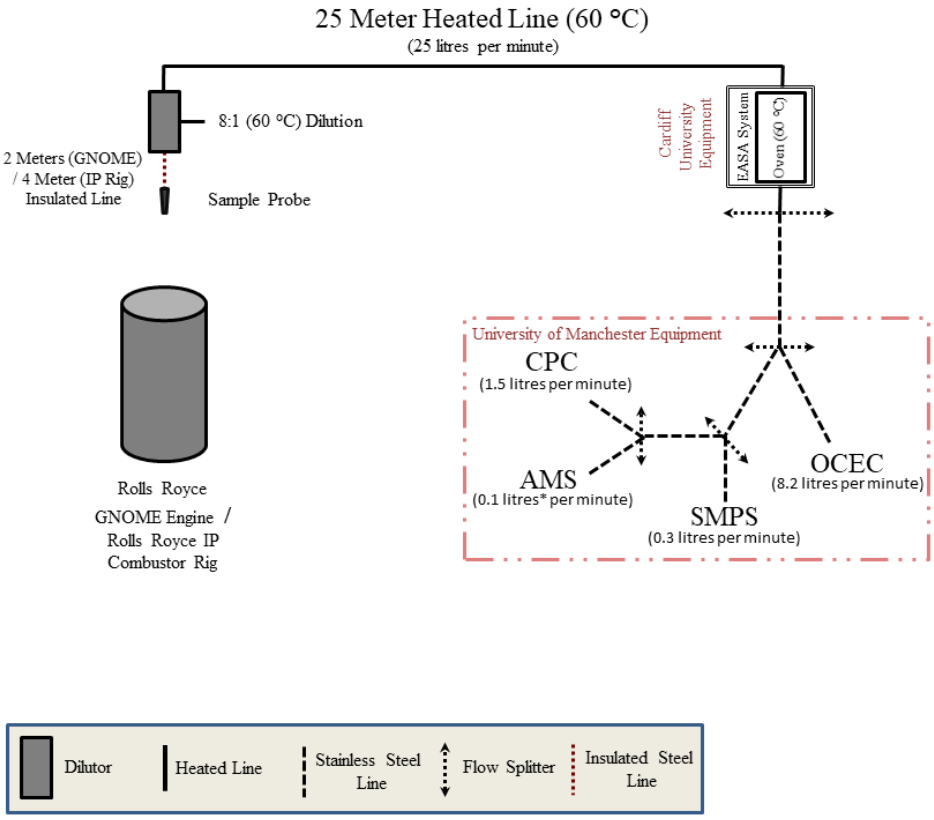

Fig.1 Schematic of experimental setup (*AMS had a flow rate of 0.072 litres per minute).

2.2 Operating Conditions

The test campaign covered a variety of power conditions for both emission sources. The Gnome engine was operated at two engine speeds, 10k & 21k Revolutions per Minute (RPM) for three runs at each condition. The IP combustor rig conditions were varied by changing combustor ΔP/P (henceforth referred to as ΔP/P), and changing the air to fuel ratios (AFR) at both the fuel injector (referred to as fuel spray nozzle (FSN) in the results) and combustor at a given ΔP/P.. Each measurement condition in this paper

is referred to by its own Test Point (TP) with respective TP number. TPs were typically ~4 to 5 minutes duration which were not enough to obtain an OCEC deposited sample above limit of quantification (LOQ). As such, seven TPs were extended to facilitate an OCEC filter acquisition. These seven TPs and their respective combustion conditions are shown in S: Table 1, and an overview of their quantity and chronological order is presented in S: Table 2. All IP rig TP results (with and without OCEC sample) are displayed in the Section 3.1 titled 'General Results', while only the seven extended TPs (with OCEC sample) were analysed with PMF with results presented in Section 3.2 titled 'PMF Analysis & Discussion'.

2.3 Data Analysis

All AMS data analysis toolkits applied within this study used IGOR 6.37 (Wavemetrics). AMS data was analyzed via the ToF-AMS data analysis software SQUIRREL v1.57H. The organic mass spectra from the experiments were subsequently analyzed with both PMF & ME-2 using the Source Finder tool (SoFi; Canonaco et al, 2013). AMS scans were 30 second averages obtained in Mass Spectrum (MS) mode. The data chosen for analysis ensured a broad range of both operating conditions and spectral differences affording an understanding of impact of flame richness, potential oxidative processes and oil / non-oil sources contributing volatile sources in the data.

As this study is concerned solely with aerosol properties, measures were taken to negate gas contribution to the AMS organic mass concentration. This was achieved by implementing condition-specific organic gas to air (N_2) ratios into the frag table (table in the SQUIRREL toolkit which calculates aerosol species by subtracting ratios of

atmospheric gases to N_2). Due to the short (<1 minute) duration of the IP rig runs without OCEC analyser sampling, the condition-specific CO_2 reading was implemented into the frag table to subtract gaseous CO_2 from the total organic mass concentrations presented in 3.1.2. For every other condition presented (those with OCEC analyser sampling), the AMS was equipped with a total particle HEPA filter, through which the sample flow could be directed. During the experiments, for each condition, the AMS sampled for at least one scan through the HEPA filter, providing a measure of the residual (missed by the original frag table corrections) gas contribution to the AMS organic matrix for each condition. Residual organic gas contribution during HEPA filter AMS scans were in the range of 0.1 – 1.2 $\mu g/m^3$ for the whole dataset when using the default frag table. In the post-processing of the data, the contributions from the major gas peaks were subtracted, those being m/z 12, 29, 40 & 44. This was conducted by calculating the ratio of each peak's residual gas (mass contribution seen during HEPA filter scan) in the organic wave to the m/z 28 signal in the 'all wave', (both gas and aerosol species)except for m/z 12, in which a ratio was calculated with m/z 44 as it is in the standard frag table. The ratios were used in the AMS data analysis software SQUIRREL v1.57H. This resulted in the residual organic mass concentration during HEPA filter AMS scans being reduced by between 1-2 orders of magnitude.

As the mass concentrations of individual m/z's are far more sensitive to gas contributions than the total concentrations, only conditions with HEPA filter gas corrections (during OCEC analyser sampling, which afforded more time) had their mass spectra examined with PMF here. All chosen organic matrices were combined to create one single dataset subsequently analyzed through both ME-2 and PMF, with all

zeroes and negative values removed prior to the processed dataset's insertion into the SoFi Graphical User Interface. The input matrices chosen comprised mass to charge ratios (m/z) ranging from 12-150 as most ions detected by the AMS in this research were within this region.

Both PMF and ME-2 were used to help evaluate lubrication oil contributions to the organic mass spectra. The methodology used for investigating oil detection is outlined in the 'Data Analysis' section of the supplementary information (SI). The outcome of this investigation is detailed in both Section 3.2.1 of the Results and Discussion and also in the SI.

The derived PMF factors were named according to their spectral features and their correlations with instrument observations, discussed in further detail in Section 3.2. References to volatility in the factor naming is based on their correlation with organic material converted to CO_2 at the lower and higher temperatures in the thermograms of the OCEC analysis, as discussed further in Section 2.4.

Ulbrich et al. (2009) noted the importance of including correlation with external tracer time series for choice of number of factors alongside Q/Qexp (which is defined in the SI of Zhang et al, 2015, as: the ratio between actual sum of the squares of the scaled residuals (Q) obtained from PMF least squares fit and the ideal Q (Qexp)) vs number of factors when choosing PMF solutions. Therefore, the appropriate factor solution of PMF was chosen through a balancing of several quantitative and qualitative metrics for viability: those being, (1) physical plausibility of the factor mass spectra, (2) correlation between factors and tracers detected by the instrumentation suite and (3) a Q/Qexp

value as near to 1 as possible without hindering the other assessed metrics.

In this study, between two and five factor solutions were appraised. The two-factor solution had a Q/Qexp value of 11.4 with 6.5 % unexplained mass. The three-factor solution decreased Q/Qexp to 4.6 alongside reducing unexplained mass to 4.2 %. The four-factor solution had a further Q/Qexp decrease to 2.7; however, the linear correlations between existing factors and external instrument tracers decreased. The five-factor solution had two near identical factors, which was assumed to be factor splitting. Alongside this, the decrease in the average variability between AMS organics and the sum of the PMF factors was only from 99.8 % to 99.5 % between the three and four-factor solution. Therefore, the three-factor solution was chosen. The residual mass concentration per scan for the three-factor solution averaged 0.26 $\mu g/m^3$ for the entire campaign.

2.4 OCEC Analyser Methodology

The OCEC Analyser's results were required to provide support for the PMF factor solution found in this study; therefore, a brief explanation of its operation and the applied analysis protocol is included in this section, additional explanation is included in the SI section under the same title. The OCEC Analyser operates via deposition of particulates on a quartz fiber filter within the instrument and subsequent exposure of the filter to a range of user-specified temperatures while in the presence of two different gas mixtures. Particles deposited on the filter are firstly exposed to an oxygen free helium atmosphere so that only OC which evaporates off the filter should be converted to CO_2 in an oxidizer oven located after the sample oven (unless there is contamination

which provides a source of oxygen, such as iron oxide; see Karanasiou et al. 2015). The deposited particle mass is then exposed to an oxygen /helium mixture (10 % O_2, 90 % He), enabling the remaining carbonaceous material to be converted to CO_2 in the sample oven, which is assigned to the EC mass. The OC analysis consisted of four temperatures, which are named OC1 up to OC4, which are outlined with their duration in S: Table 3. The OC converted to CO_2 at specific temperatures are used to infer potential volatility of certain PMF factors in the PMF results. Semi-continuous thermal-optical OCEC analysis is characterised further by other studies (Bauer et al, 2007).

In this study, the selected temperature profile for the OCEC Analyser was a modified NIOSH 5040 protocol. It has a higher maximum EC temperature of 930 °C (developed for gas turbine PM measurements) and an extended burn time duration (duration of the highest temperature during the OC phase) details are provided in S: Table 3. The choice to both extend the burn time and raise the highest EC phase temperature was to accommodate the conditions for the emission sources used in this study. Some of the OCEC Analyser thermograms did not to appear to have completed their removal of material at OC4 (as the CO_2 value was still rising) on tests prior to those presented here, so the length of the OC4 phase was extended. Furthermore, OC4 had what appeared to be early EC burn-off in the OC phase, as laser transmission exceeded its starting value, indicating refractory material other than Pyrolyzed Carbon (PC) was converted to CO_2. This is reported in subsection 3.1.3 within the general results. As an extra measure for data quality assurances for this issue, all thermograms were analyzed further using the AVEC method - used to determine the appropriate split times - as developed by Nicolosi et al. (2018). Some thermograms' CO_2 readings did not start at zero and had either

positive values or negative values due to a baseline offset. To adjust their baselines, simple addition or subtraction to these values were applied to bring their baselines to zero which ensured comparability between each thermogram. The same value was applied to all CO_2 values in the thermogram and therefore did not affect the trends within them.

3. Results and discussion

Three primary results were obtained: (1) general instrument results measured across operating conditions from both emission sources, which are presented in Section 3.1; (2) factor analysis of the AMS organic mass spectra obtained during the OCEC Analyser's sampling time; and (3) their correlations with instrument tracers. The latter two result types are presented in Section 3.2.

3.1 General Results

Across the Gnome and IP rig conditions, a wide range of results were observed across several variables. The Gnome 10k RPM conditions exhibited higher total organics detected by the AMS (39 - 61 μg/m^3) compared to the 21k RPM conditions (24 – 29 μg/m^3) (S: Table 4). The first 10k RPM condition displayed a decreasing total organic concentration scan-to-scan and resulted in a higher AMS mean average organic concentration - across the condition - than the latter two 10k RPM runs (S: Table 4; S: Figure 6). This may have been due to engine instability after initial switch on, which is supported by PMF results presented in Section 3.2. Despite this, the results showed a near identical average organic mass spectra for all 10k RPM runs. The three 21k RPM condition's AMS organic mass concentrations on the Gnome engine were stable throughout. AMS PToF size distributions showed all organics and sulphate from both sources observed here were present in the soot mode (See SI section 'PToF Results'). It was concluded that this material was either condensed or agglomerated on a larger soot surface which allowed delivery to AMS in a size range with higher transmission efficiency.

3.1.1 Gnome Engine

The AMS average mass spectra at both 10k RPM & 21k RPM conditions possess two homologous series of 14 atomic mass unit intervals starting with m/z 27 & 29 (Figure 2). These are a series of ions produced by straight chain alkanes (saturated aliphatic hydrocarbons) at $C_nH_{2n+1}^+$ and then less commonly at $C_n2_{n-1}^+$ and are named the $\Delta = 0$ & 2 series by McLafferty and Turecek (1993). Lobo et al. (2012) showed using gas

chromatography analysis of Jet A1 fuel, that typically the fuel's mass was mainly made up of saturated aliphatic hydrocarbons with carbon numbers of 8, 10, 12 & 14, the masses of which are shown in S: Table 5. Yu et al. (2012) also noted that kerosene-based aviation fuel is composed primarily of a combination of hydrocarbons with a carbon number from 8 - 16, citing decane ($C_{10}H_{22}$) as a suitable reference for jet fuel. Due to decane's prominence in jet fuel, and its similarity in mass spectrum to the other compounds which specifically make up Jet A1 fuel (S: Table 5), it is used as a reference for unburnt fuel in this work. With this considered, qualitatively speaking, OA emitted during 21k RPM conditions appear to be largely made up of straight chain alkanes, which originate from unburnt fuel, due to the decane similarity (Figure 2). This may be explained due to a higher fuel flow rate at the higher engine speed. Alongside this, there appears to be a paucity of other compounds present in this aerosol phase at 21k RPM conditions, given that each peak in the alkane ion series contributes much greater proportions than those at 10k RPM. 10k RPM conditions had a higher diversity of mass signals in its spectra with a comparatively higher signal in the $\Delta = 0$ ion (C_nH_{2n-1}) in the $\Delta = 0$ & 2 series (e.g. m/z 27, 41, 55 & 69) alongside that of the $C_nH_{2n}^+$ ion. An increase in the $C_nH_{2n}^+$ and $C_nH_{2n-1}^+$ has been shown to be symptomatic of unsaturated aliphatic hydrocarbons (McLafferty & Turecek, 1993). Alongside these, the 10k RPM spectra contained the homologous ion series of phenylalkanes, of masses m/z 77, 91, 105 (McLafferty & Turecek, 1993). Reductions in temperature and combustion efficiency that are seen at lower engine speeds (McKinney & Hoke, 2013) appear to have allowed these species to enter the PM phase, which are not seen at the higher engine speed. These aerosol measurements reflect those seen in gaseous emissions testing, where results have shown that temperature changes were responsible for emission changes of

certain organic species, including aromatic compounds (Yelvington et al, 2007). This in turn correlates with the aerosol processes observed here within this ICAO compliant sampling setup, as the Gnome's exhaust gas temperatures during 10k RPM conditions are approximately 400 ºC, while at 21k RPM conditions they are approximately 500 ºC.

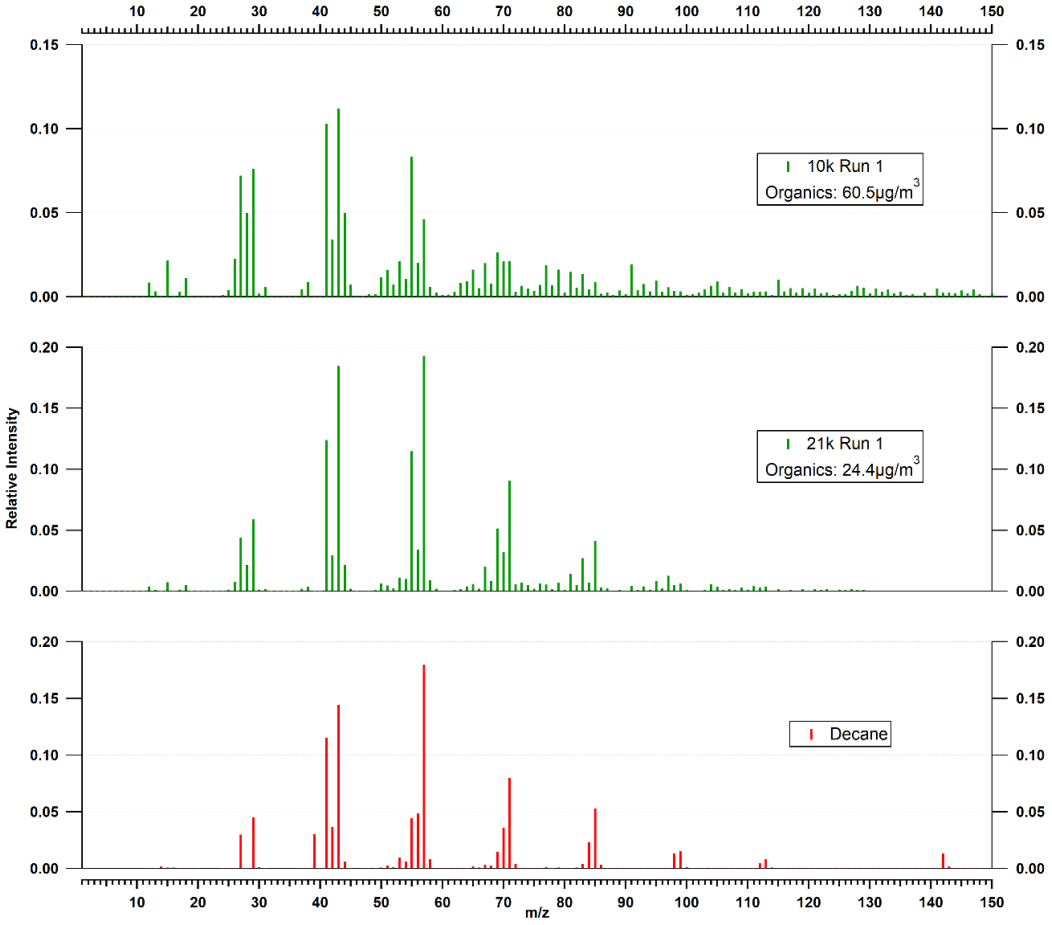

Fig.2 Gnome average AMS mass spectra taken from 10k Run 1 (Top), 21k Run 1 (Centre), and a decane mass spectrum (Bottom). Decane mass spectrum is taken from NIST webbook.

Evidence of increased oxidation of hydrocarbons during 10k RPM conditions relative to those at 21k RPM were shown in the ratio between AMS-detected mass markers m/z

44 & 43 (Figure 2, referred to as f44/43 for brevity). f44/43 is used to determine the level of oxidation in OA in atmospheric studies (Ng et al, 2010) as m/z 44 is resultant of thermal decarboxylation of carboxylic acids which produces CO_2+ ions in the AMS because of this process. This process is seen in other combustion source studies (e.g. Elsasser et al., 2013). f44/43 at 10k RPM conditions ranged between 0.36 - 0.44, whilst at 21k RPM they ranged between 0.08 - 0.11, indicating that aerosol detected during 10k RPM conditions had higher levels of oxidation compared to those at 21k RPM conditions. Corresponding OCEC analyser data indicated that aerosol volatility was lower during 10k RPM conditions relative to that at 21k RPM conditions. In the OCEC analyser thermograms, the OC mass converted to CO_2 was distinctly higher in the OC1 (310 ºC) and OC2 (475 ºC) phases during 10k RPM conditions than those at 21k (Figure 3). This implies that the organic compounds emitted at the lower engine speeds (e.g. 10k RPM) have lower volatility than those emitted at 21k RPM.

Sulphate is expected in the emitted aerosol, as it has previously been shown to originate from and correlate with the quantity of the fuel's sulphur content (Timko et al, 2010; Moore et al, 2015). Sulphate has an influence on the aerosol number generated (Anderson et al, 1998) and mass concentrations (Onasch et al, 2009). Here, it was only during 10k RPM conditions that the AMS detected sulphate from the Gnome engine (S: Table 4). As discussed, these sulphate values are likely to be under-reported due to both line and AMS instrument losses within the nucleation mode (<20nm) in which sulphate aerosol has previously been observed (Anderson et al, 1998; Onasch et al, 2009). PToF size distributions showed sulphate was in the soot mode. This must have agglomerated or condensed onto the soot surface, but despite this, the mass concentrations of sulphate

during Gnome engine conditions did not correlate with those of elemental carbon, as was observed by Timko et al (2010). Sulphate precursor evolution simulations have shown that at idle conditions, when an engine is operating at the lowest pressure and temperatures, SO_3 to H_2SO_4 conversion was a significant fraction of SO_x oxidation (Lukachko et al, 2008). Laboratory experiments have shown the $SO_3 + H_2O$ to H_2SO_4 pathway to have a strong negative temperature dependence (Jayne et al, 1997). As mentioned, the Gnome engine exhaust gas temperatures are thought to be approximately 400 °C at 10k RPM and 500 °C at 21k RPM, though were not measured here. Furthermore, high SO_2 to SO_3 conversion in older design engines (such as the Gnome engine used here) has been shown to occur in their combustors at both idle and takeoff conditions (Lukachko et al, 2008). Hence, we suggest that sulphate was only observed during Gnome 10k conditions for two reasons: firstly, due to possibly higher conversion efficiency of SO_2 to SO_3 during these conditions; secondly, due to lower exhaust gas temperatures during 10k RPM than those during 21k RPM which could have facilitated better conditions for the $SO_3 + H_2O$ to H_2SO_4 post combustion reaction in the four meters from engine exit to the sampling probe. After the four meters distance to the sampling probe, this formation was prevented from occurring further in the 25-meter sampling line by the dry nitrogen dilution flow, reducing the water vapor concentration, which has shown to reduce first-order decay rates of SO_3 (Jayne et al, 1997). Influence of the setup on both outlined chemical reactions may have been negated had greater sampling distances been used, as total sulphate mass EIs (both nucleation and soot mode) have been shown to be stable across operating conditions at 30 meters (Onasch et al, 2009) presumably as the influence of exhaust gas temperature diminishes across such distances.

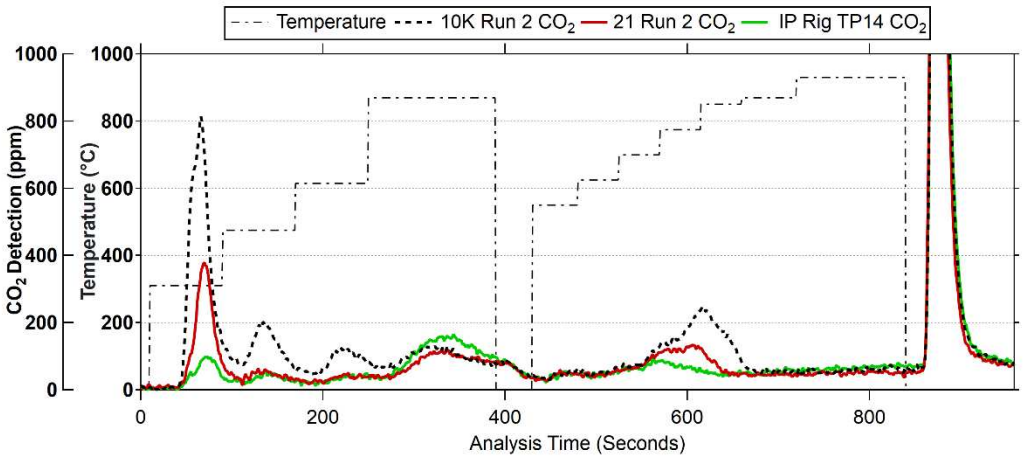

Fig.3 Merged thermograms for 10K RPM Run 2, 21k RPM Run 1 & IP Rig TP 14. Gnome 10k RPM run 2 was included as its thermogram is representative of the third run of the same condition. Gnome 21k RPM run 1's thermogram is representative of the other two repeats at this engine condition. IP rig TP 14 is included as the peak-to-peak ratio on its thermogram is representative of most other thermograms produced at other IP rig TPs.

3.1.2 IP Rig

The IP combustor rig offers a broad range of engine-relevant operating conditions via a range of FSN AFRs and combustor inlet air temperature and pressure conditions. Secondary air (filtered compressed air) is introduced perpendicular to the flame with the aim of quenching (cooling and diluting) the flame emissions prior to burnout within the combustor. This allows analysis of FSN emissions. However, the sampled emissions will not have undergone the subsequent high temperature oxidation process that occurs in commercial gas turbine engine combustors.

For a single FSN, the relationship between FSN AFR and combustor AFR and vPM is shown in Figure 4. LII-detected EC mass concentrations at a given ΔP/P decreased with FSN AFR as conditions became increasingly lean (Fig. 4a). With increasing ΔP/P values, the gradient of the line against FSN AFR decreases, with increasing scatter at low ΔP/P as indicated by their regression coefficients. Lower combustor ΔP values are associated with higher primary zone equivalence ratios in combustor rigs, previously attributed to poor atomisation resulting from low atomiser air mass flow (Rye et al, 2012). Higher ΔP results in more quench air penetrating to the centre of the flame zone and creating better mixing, which is seen here to reduce EC mass concentrations, this increase in combustion efficiency is furthered by increasing the FSN's AFR. Similar observations were made by Fujiwara et al (2020) in a rich-quench-lean combustor, with maximum nvPM EIs observed at combustor AFRs of 65, those observed here were observed at combustor AFRs ranging 55-60, dependent on the ΔP/P. Increasing nvPM EI number and mass have been observed on a CFM56-7B26/3 engine when using the same sampling methodology applied here (Lobo et al, 2020).

Organic and sulphate mass concentrations are plotted against LII-detected EC mass concentrations (Fig. 4b) and both positively correlate. As discussed, this may indicate that both exist on the surface of EC nvPM particles as either condensation or agglomerated smaller nucleated material. This would enable the material to be in sizes with higher AMS transmission efficiency.

A strong inverse relationship between sulphate mass concentrations and combustor AFR is observed, with the highest concentrations at the richest (lowest AFR) combustor conditions (Figure 4c). As in the case for EC, there is some variation at a

given AFR which is explained by ΔP/P, with higher ΔP/P being associated with lower sulphate mass concentration. This again is likely due to improved mixing with higher ΔP/P; however, this is less clear at combustor AFRs greater than 80 when conditions become lean and fuel flow is lower (Figure 4d). On first inspection, the sulphate trends seen here in the IP Rig are the opposite to that which is seen in the Gnome engine regarding temperature influence. The sulphate increases exponentially with T40 temperatures (S: Figure 3). However, the piccolo probe cools all sampled air down to the approximate exhaust gas temperatures which would be seen during Gnome 10k conditions and does so for all IP test points. With this cooling, it is likely that sulphate forms as a function of quantity of fuel (and therefore sulphur within fuel) injected into the rig (Figure 4d) and internal combustion processes as opposed to exhaust gas ones. Simulations of SO_3 conversion efficiencies have been shown to be highest in combustor rigs in conditions equivalent to take-off and idle conditions (Lukachko et al, 2008). In full scale engines at distances of 30 meters, sulphate emission mass indices in the soot mode have also been observed to increase with engine power, and therefore in conditions which are richer (Onasch et al, 2009). These observations match those seen here. It is therefore hypothesised here that the usage of both the quench air and water-cooled sampling probe for the IP Rig conditions negated the hypothesised post combustion temperature effects in the Gnome engine.

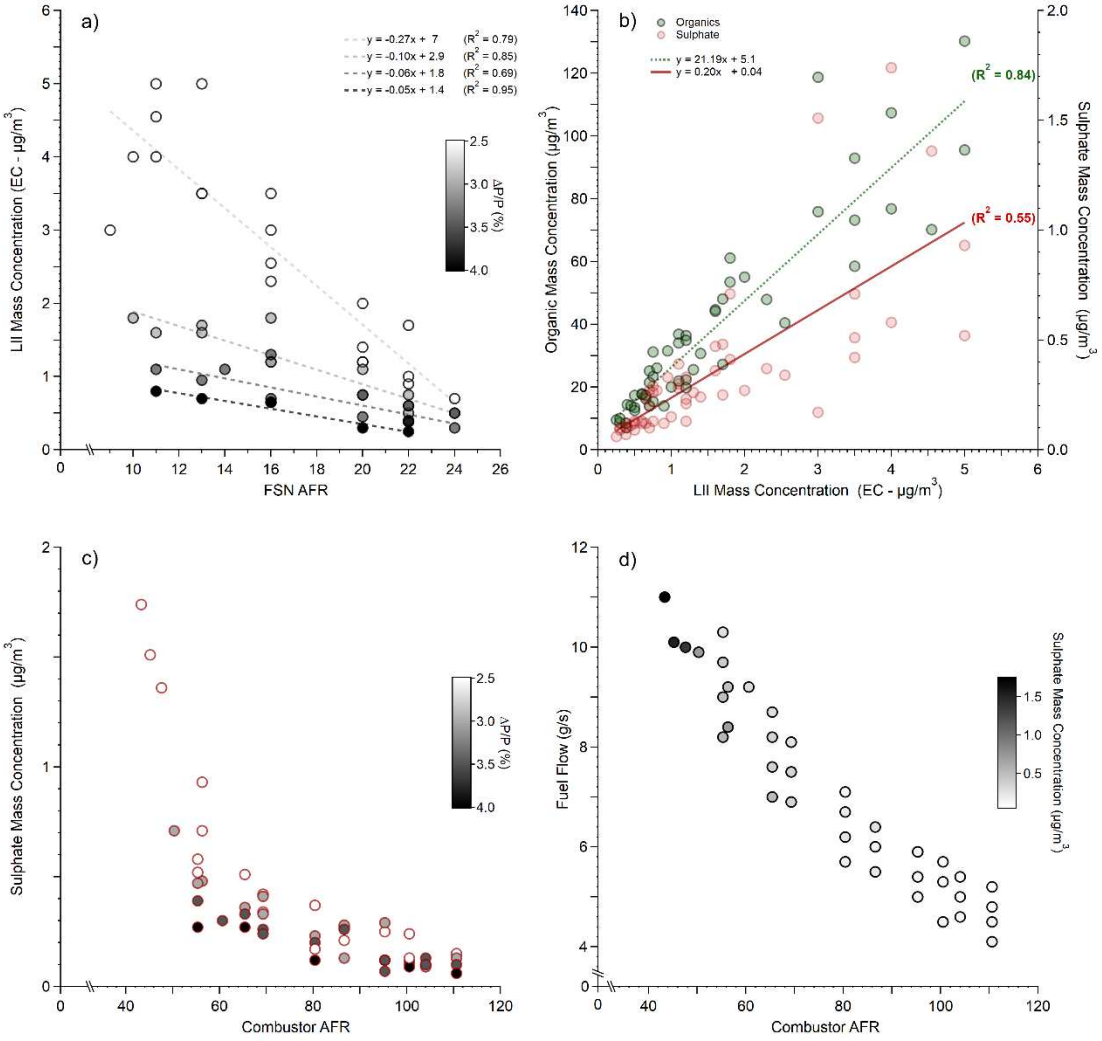

Fig.4. IP rig emission data. All presented data is from outside the OCEC Analyser's sampling phase to ensure comparability between sample flow rates, therefore does not include the conditions later analysed by PMF.

4a – LII-measured EC mass concentrations versus FSN AFR. Linear regression lines are for the four different ΔP/P values (from top to bottom: 2.5%, 3%, 3.5% and 4%) of the same colour indicated by the colour scale. The legend of the trend lines rank orders them in ascending order.

4b - AMS Sulphate and Organics as a function of LII mass concentration. Linear regression lines are for organic (dashed green) and sulphate (solid red) mass concentrations.

4c - AMS-measured sulphate mass concentration versus combustor AFR.

4d – IP Rig fuel flow rates measured against combustor AFR, markers shaded by their sulphate mass concentrations.

3.1.3 OCEC Analyser Thermograms

Every thermogram showed signs of OC undergoing pyrolysis and producing PC, which was visible by the decreasing laser transmission during the inert phase of each sample's analysis. This is normal and expected in thermal-optical analysis, however early burn-off of EC in the inert phase is not. Indicated by the instrument's laser exceeding its starting value during the OC phase, six out of the eleven thermograms examined here appeared to show early burn-off of EC during the highest temperature of the inert section of analysis. For example, in IP Rig TP23, the laser's transmittance was 2.5x higher at the end of the inert phase than it was at the beginning of the analysis (S: Figure 4). The paucity of oxygen during this phase should prevent EC burn-off however the high temperature used in the NIOSH protocol (870 °C) has been shown to produce early EC burn-off in prior study (Subramanian et al, 2006). Subramanian et al (2006) showed that reducing the OC4 temperature for a sample's analysis can reduce this early burn-off of EC, and future studies should examine this in a gas turbine context and consider a lower OC4 temperature.

To subtract early EC evolution from thermogram analysis, any CO_2 detected

after the laser transmission had increased above its starting value for that condition was not included in the OC4 readings presented here unless otherwise stated. Despite this influence, every thermogram produced CO_2 which only evolved at the highest temperature (870 °C) of the analysis (S: Figure 5). This may have been low volatility OC in the PM phase, which has been detected in prior aircraft emissions testing, requiring temperatures between 350°C - 500 °C to volatilise (Petzold et al, 2005). Gaussian fit analysis on a thermogram with an operating condition with a low smoke number and a high organic matter from the SAMPLE I project showed a peak CO_2 peak at ~425°C but no increase in laser transmission, indicating a low volatility OC peak (EASA, 2009). The possibility of PC production influencing the OC4 peak in this paper's data cannot be ruled out, though the rising OC4 peak did coincide with changing AMS detected composition and correlate with PMF factors in which the spectral characteristics also indicate reduced volatility, which is discussed in section 3.2.3. If the OC4 CO_2 was produced due to low volatility OC products - given that a temperature of 875 °C was required to volatilise this material - it opposes the assumption that nvPM is synonymous with soot or EC. If OC, current definitions would class this as nvPM as it requires temperatures greater than 350 °C to volatilise, while it may remain undetected by the nvPM mass concentration analysers currently applied in standards testing. Further research is needed on this issue.

3.2 PMF Analysis

3.2.1 Oil Contribution

Steps were taken with both PMF and ME-2 to evaluate the levels of lubrication oil contributing to the OA mass spectra, as detailed in both the SI methodology and SI results section. The analysis showed that no oil was detected or it was non derivable. Four possible explanations are provided: (1) No oil was present in the extracted sample, supported by Yu et al's (2012) m/z 85/71 method due to the location of the probe relative to the vent; (2) The oil existed in diameters below the AMS's detection limit (30nm-50nm); (3) The oil underwent thermal processes within the engine itself and therefore is chemically altered from the mass spectra taken from the oil which was extracted directly from the Gnome engine's oil storage; (4) that the oil made up less than 5 % of the organic mass, which PMF has been shown to be ineffective at detecting such quantities (Ulbrich et al, 2009).

3.2.2 Positive Matrix Factorisation Overview

Having identified that lubrication oil contribution was either negligible or non-derivable, the usage of a-priori evidence of the oil target factor was disregarded and the remaining factors contributing to the organic mass were examined through PMF. A three-factor solution was selected as discussed in the methodology.

The three factors are shown in Figure 5 and their mass markers are presented in S: Table 6 for further reference. Each factor's spectral features are described further in Section 3.2.3 alongside their correlation with instrument tracers, which provide support for the

PMF solution. The factor's relation to operating conditions is later discussed in Section 3.2.4.

The solution's unexplained mass concentrations, measured by the ratio of the summation of all three factors' mass concentrations to the AMS' organic mass concentration showed consistently nominally identical values throughout the data (S: Figure 7 & S: Figure 8). The differentiation from PMF total mass concentrations to the total AMS organic mass concentration being from 7 % below and 15 % above for only one AMS scan (S: Figure 8). The three factors were named Alkane Organic Aerosol (AlkOA), Semi-Volatile Oxygenated Organic Aerosol (SV-OOA) & Quenched Organic Aerosol (QOA) and are presented in Figure 5.

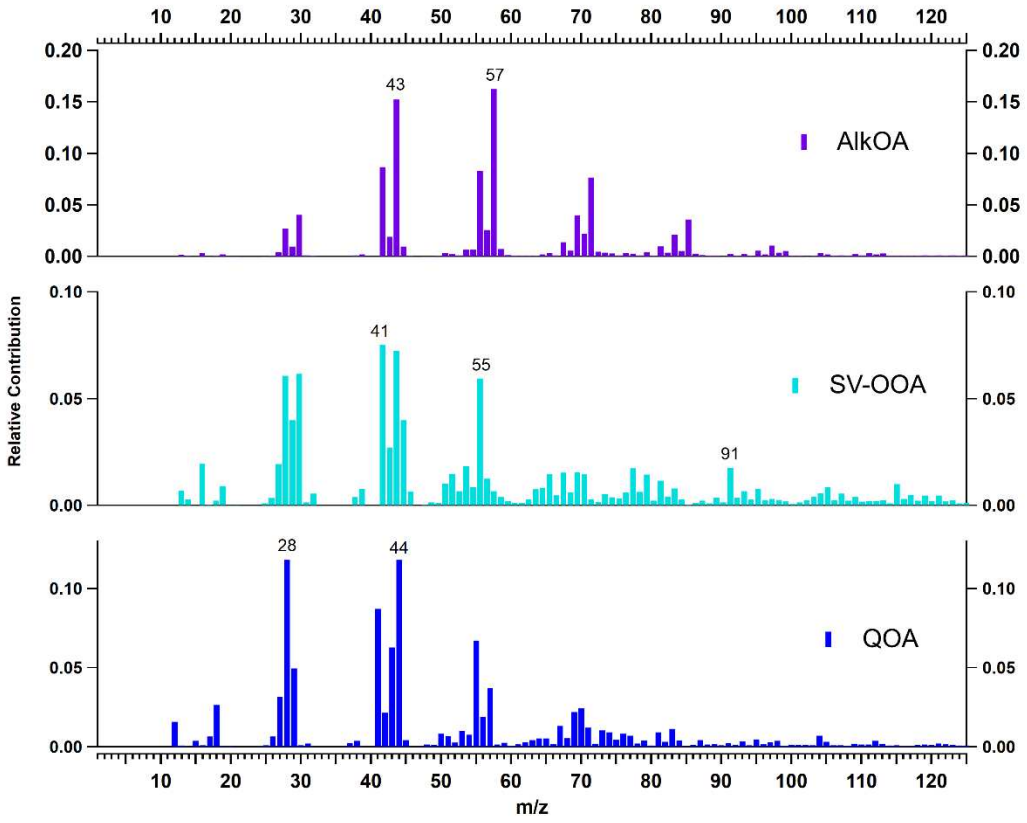

Fig.5 PMF Factors: Alkane Organic Aerosol (AlkOA), Semi-Volatile Oxygenated Organic Aerosol (SV-OOA) and Quenched Organic Aerosol (QOA). Important mass markers are numbered.

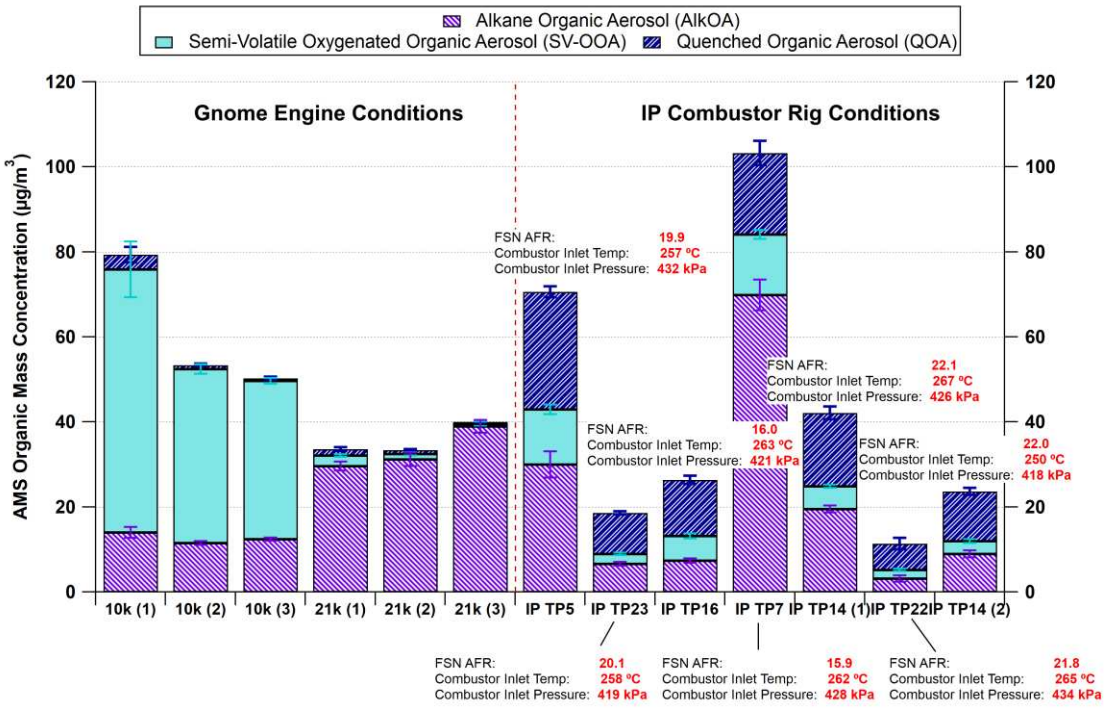

Fig.6 PMF Factor's Mass Contributions. Error bars show one standard deviation. IP rig TPs are not in chronological order and have been reorganized so that TPs are next to those with two variables within a comparable range (TP5 & TP23; TP16 & TP7; TP14 (1) & TP22), while TP14 (2) has two variables changed from all other TPs. For a chronological view with individual AMS scans, see S: Figure 7.

3.2.3 PMF Factors

AlkOA - The first factor was named AlkOA due to its straight chain alkane fragmentation pattern. As discussed in the 'General Results' section, decane served as the unburnt fuel marker. The decane mass spectrum values were taken from NIST webbook (NIST Mass Spectrometry Data Center, 1990), normalized, and plotted against the AlkOA factor (S: Figure 9 & S: Figure 10; $R^2 = 0.91$). Due to the observed

similarities, and decane's prominence in Jet A1 fuel (Lobo et al, 2012), AlkOA is concluded to be unburnt fuel. The AlkOA factor was seen across all operating conditions from both sources (Figure 6), as would be expected as it is the constant between both the emission sources and all operating conditions. In-situ measurements taken from emitted plumes at distances of 30 meters have also detected OA containing incomplete combustion products or partially burned fuel (Timko et al, 2010).

During Gnome conditions, AlkOA correlated with EC (Figure 7) detected by both the OCEC Analyser ($R^2 = 0.92$) and LII ($R^2 = 0.78$). For IP rig conditions, AlkOA and LII-detected EC had a strong correlation (Figure 7; $R^2 = 0.90$). For OCEC data, AlkOA and EC had moderate correlation ($R^2 = 0.62$). When the OCEC-detected EC and AlkOA data from both emission sources are combined, the combined linear correlation decreases (Figure 7: $R^2 = 0.58$). This implies that while the variables governing EC and AlkOA production in each emission source are related, they are not equal between engine technologies.

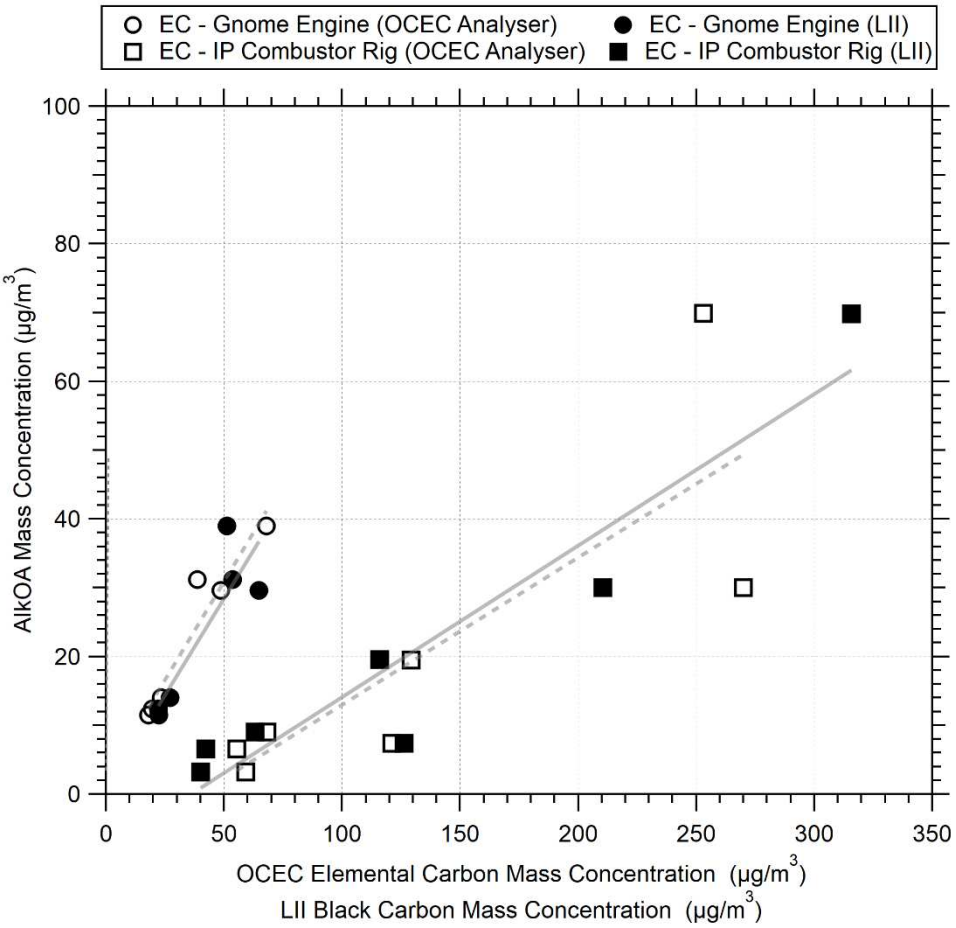

Fig.7 AlkOA plotted against elemental carbon mass concentrations detected by both the OCEC Analyser and the LII. The AlkOA chemical factor correlated with elemental carbon concentrations from two instruments. The strength of the relationship changed between emission sources. Please note that LII values are without dilution correction so that values are comparable with OCEC values. Further presentation of LII data in section 3.2.4 are dilution corrected values.

SV-OOA - The second factor detected by PMF is named in this paper as 'Semi Volatile-Oxygenated Organic Aerosol' (SV-OOA). There was strong correlation between the mass concentrations of SV-OOA and AMS-detected Sulphate ($R^2 = 0.99$). Its naming

is due to its correlation with OC detected at the lowest temperature settings in the inert phase (OC1) of the OCEC analysis (S: Figure 11). In the Gnome, SV-OOA correlated with all OC temperature stages, though the regression coefficients and gradient were highest with OC1 (S: Figure 11; R^2 = 0.99; with one anomaly from Gnome 21k conditions removed, as its OC1 value was greater than the two condition repeats by a factor of two) and the gradient decreases with each temperature stage, until OC4, where it increases. In the IP rig SV-OOA also correlated with every temperature stage, but linear regression shows the relationship becomes weaker with increasing temperature (R^2 values: OC1 = 0.81; OC2 = 0.53; OC3 = 0.32; OC4 = 0.55). Despite the increase in the regression coefficient for OC4, the mass of OC4 was better determined by QOA mass, as discussed in its section. This may imply that the average volatilities of the molecules detected within the SV-OOA factor are lower than those of QOA. It is acknowledged that there are few datapoints analysed by the OCEC Analyser here, though the reduced *f*44/43 in SV-OOA's mass spectrum relative to that of QOA's would also indicate lower volatility based on prior study of organic aerosol (Jimenez et al, 2009).

SV-OOA possessed the phenylalkane ion series outlined in the general results (McLafferty & Turecek, 1993). The mass concentration of m/z 91 from the average AMS mass spectra (pre-PMF analysis) very strongly correlates with the PMF-processed SV-OOA factor's total mass concentration (R^2 = 0.99), which is assumed to be a toluene ion. Another aromatic marker within SV-OOA's spectral features, is that of m/z 115, which has been showed to be (>95 %) contributed by an Indene (C_9H_8) ion in prior aircraft aerosol research (Timko et al, 2014). Considering this, alongside its higher

f44/43 than AlkOA, the SV-OOA factor is consistent with the presence of hydrocarbons containing oxygenated and/or aromatic groups. This aerosol product may have formed rapidly within the 2-4 meters applied in this study as aromatic chemical groups have been observed in the PM phase at distances of 30 meters and greater (Timko et al, 2014). Such rapid formation could have implications for plume or local air quality modelling, however it must be acknowledged that the dilution stage may have facilitated the condensation of this chemical group, although the trends (discussed more in Section 3.2.4) with engine operating conditions match gas phase aromatic trends seen at greater distances (Yelvington et al, 2007).

QOA - The third factor is termed Quenched Organic Aerosol (QOA) due to its occurrence only during IP rig conditions (Between 20-50% of mass concentrations; With exceptions of 1-4% of mass during the Gnome 10k conditions). This is hypothesized here due to the quench air applied after the combustor flame in the IP rig, and is discussed further in section 3.2.4. QOA correlated with all OCEC analyser OC at each temperature stage, though with the inverse of that seen with SV-OOA (S: Figure 11; R^2 values: OC1 = 0.65; OC2 = 0.69; OC3 = 0.77; OC4 = 0.85). The increasing regression coefficient at each temperature stage may imply a lower volatility than that of SV-OOA. This is reinforced by QOA's spectral characteristics, as this factor is characterized by the highest f44/43 of the three factors, implying it is the most oxidized aerosol factor (Ng et al, 2010). Given that the QOA factor has a high f44/43, it would be expected to have lower volatility than the SV-OOA factor due to the greater degree of oxidation (Jimenez et al, 2009). This is reflected in the IP Rig's OCEC analyser thermograms, shown by the increasing regression coefficients with each increasing

temperature stage. It is acknowledged however that PC is produced at these higher temperatures, and this could influence the presented OCEC Analyser-detected CO_2 values, although this would not explain the coinciding with changes in spectral characteristics in the AMS alongside the correlation with QOA's PMF mass concentration.

3.2.4 Compositional Trends of PMF Factors

The usage of PMF confirmed the aforementioned spectral observations in the general results and enables for the differentiation of mass concentration contribution between factors at given conditions, which was challenging prior to the application of this analysis technique. There may be uncertainty around these separations, however the outlined instrument tracers that correlate with each factor provide validation. The role of the sampling system regarding compositional changes between conditions examined here is assumed to be of lesser importance due to the maintenance of flow rates and dilution ratios throughout testing.

Gnome engine OA emissions were almost entirely composed of AlkOA and SV-OOA, with small contributions of QOA in the first 10k RPM run (decreasing from 8% in first AMS scan of this condition to 4% in the final: S: Figure 7). It is not immediately clear as to why QOA appears at the beginning of the run, however it decreases to near-zero contributions in the latter two 10k RPM conditions. The higher mean average mass concentration in the first 10k RPM run was almost entirely due to greater SV-OOA presence. This was possibly due to a lower combustor temperature at the start of this condition, requiring more time to reach an equilibrium. This is supported by the

appearance of SV-OOA during the first and second 21k RPM conditions, with SV-OOA averaging at 7% of total organic mass concentration during the first condition, decreasing to 4% for the second, and finally 1% contribution in the third. Aside from these two differences, the composition remained approximately stable across the latter two repeats of 10k and 21k RPM Gnome conditions.

During 10k RPM conditions, OA mass concentrations were composed entirely (>96%) of SV-OOA and AlkOA with SV-OOA ranging 74 – 78% of the total. 21k RPM conditions had OA mass concentrations that were composed of between 88 - 98% AlkOA, with an increase in AlkOA mass concentration compared to 10k RPM conditions. As AlkOA is assumed to be an unburnt fuel marker, increased fuel flow rate at higher engine speeds would explain these compositional changes. If it is assumed to be largely aromatic in composition based off its spectral characteristics, higher SV-OOA mass concentrations during 10k RPM conditions can be explained by lower combustor temperatures. As mentioned previously in the 'General Results', the higher temperatures associated with higher engine speeds (McKinney & Hoke, 2013) appear to have either improved combustion efficiency or increased temperatures in the engine exhaust gas temperatures, sufficiently supressing the SV-OOA factor entering the PM phase. This is supported by gas-phase aromatic trends outlined earlier, which have shown gas phase aromatics to be disproportionately emitted at lower power settings, with ambient temperature having most effect on variation on their mass, even masking effect of plume age (Yelvington et al, 2007). This gas-phase aromatic trend has also been seen in gas-phase PTR-MS results in a similar ICAO compliant system (Kiliç et al, 2018). Mass spectra of OA taken at distances of 30 meters during idle conditions in

the nucleation and soot modes have shown more characteristic aromatic markers during 4% thrust than those taken at 85% (Yu et al, 2019). These observations agree with those presented here (Figure 5; S: Figure 7; S: Figure 9), as SV-OOA appears to contain hydrocarbon components with aromatic groups and were found during Gnome engine conditions associated with lower combustor temperatures (10k RPM). This shows that certain aromatic compounds can be found in the PM phase at near-engine exit distances using the ICAO compliant system. Many studies have shown little to no organic speciation in prior study at exit plane conditions (Timko et al, 2010; Timko et al, 2014). Interestingly, during the Gnome's 10k RPM conditions, the ratio between SVOOA to AlkOA in the OA was approximately four to one. Similar aromatic to aliphatic ratios have been observed in PMF analysis of OA taken from a CJ61O8A engine at much greater distances (Timko et al, 2014). This may indicate that the ICAO compliant EASA nvPM system sampling from near-engine exit captured some aliphatic and aromatic groups and the ratios between them found in the PM phase in aged plumes, despite the shorter distance from the examined sources used here, possibly due to lower engine thrust. However, these smaller distances may result in under-reporting aromatic aerosol mass in smaller size ranges, as aromatic mass markers have been found in the nucleation mode at idle conditions at 30 meters distance (Yu et al, 2019), while no organic nucleation mode was detected here. Future studies of vPM using a similar methodology applied here should take this potential bias into consideration.

All PMF factors during IP combustor rig conditions positively correlated with EC mass concentrations (Figure 8) which in turn rose with lower FSN AFRs and lower ΔP/Ps when adjusted for AFR. This gives further indication that all organics existed on the

soot surface. AlkOA and SV-OOA factors mass concentrations correlated more strongly with those of the LII-detected EC (Figure 8, R^2 = 0.89 and 0.94, respectively) than that of QOA (R^2 = 0.57). Few clear operating trends were found for QOA's mass concentrations, likely due to its reliance on soot surfaces to act as a delivery system to the AMS. However, the ratio of QOA mass concentration to that of LII-detected EC mass concentration (QOA/EC) increases as conditions become leaner in both the injector and combustor (Fig. 8d). Higher QOA/EC also correlated with higher ΔP/P and total air flow. The QOA/EC ratio increased with total air flow, however combustor AFR was the best independent variable to measure against (Fig. 8d). The dashed trendline in Figure 8d shows the linear regression analysis for all conditions (R^2 = 0.74) though one condition had much lower total air flow than the other conditions and when it was removed, the linear regression coefficient was raised (R^2 = 0.87). It is because of this relationship that it is suggested that the QOA factor is formed by the IP rig's quench air flow. As discussed, QOA is likely the most highly oxygenated factor due to having the highest f44/43, which is a measure of oxidation in aerosol science, as it represents thermal decarboxylation of carboxylic acids (Ng et al, 2010). With a higher f44/43, one would anticipate lower aerosol volatility (Jimenez et al, 2009), which is reflected in the OCEC thermograms with QOA's correlation with detected OC4 mass. Previously, PTR-MS results of organic gases have shown primary volatile organic compounds (VOC) to become increasingly composed of carboxylic acids as oxidation products are increased in an ageing chamber, while used in conjunction with an ICAO compliant setup similar to that used in this work (Kiliç et al, 2018). Considering this, alongside the correlation between QOA/EC and increasingly lean combustor conditions and total air flow, we hypothesise that the quench air in the IP rig caused organic condensation to undergo

similar aerosol chemical processes to that of the ageing chamber by Kiliç et al, 2018. This would explain the paucity of QOA detected during the Gnome conditions, and the high percentage contributions (20-50%) to mass concentrations during IP rig conditions only. This finding could have implications for future combustor rig vPM testing.

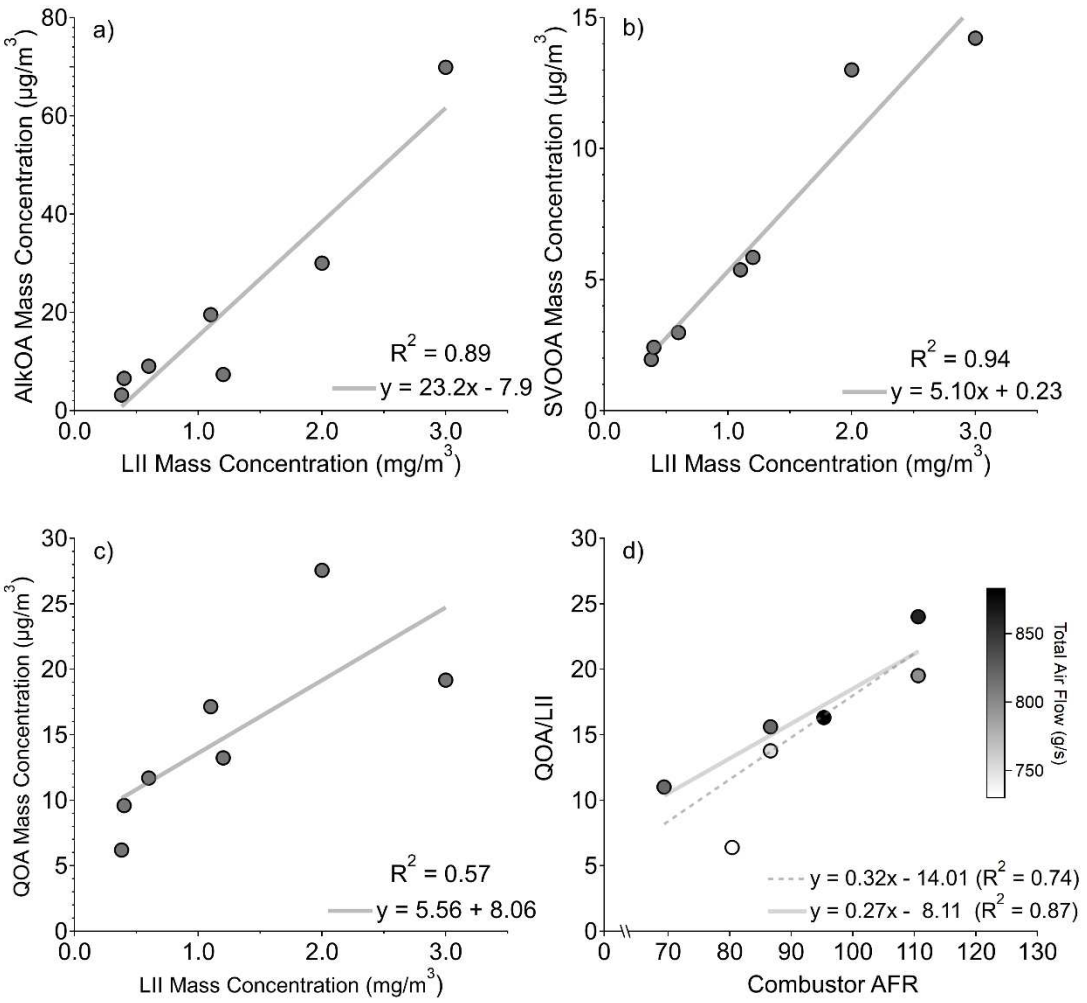

Figure 8. IP rig operating conditions and aerosol composition examined only during the seven conditions analysed during the PMF analysis. a) AlkOA concentration correlates with EC mass concentration, as does b) SV-OOA mass concentration, presumably as they are both condensates and/or agglomerates on the surface of EC surfaces. c) QOA also correlates, though less well than the other two factors. d) QOA per unit LII EC mass concentration was well explained by increasingly lean conditions in the IP rig.

4. Conclusion

The ME-2 & the PMF algorithms were successfully used to separate OA chemical groups sourced from two aircraft emission sources using the ICAO compliant-certified nvPM sampling system. The samples were examined for lubrication oil contributions to the organic matrices, and it was concluded that oil was either negligible or simply not distinguishable from other organic factors in the dataset. Several hypotheses for this were provided. The remaining organic matrices were separated into three factors; one being from unburnt fuel, signified by its Alkane content (AlkOA) and two being from oxidised hydrocarbons (SV-OOA & QOA). Total organic mass concentrations were shown to decrease with higher engine speed in the Gnome engine, similar to trends shown in gaseous emissions. The same was observed for those of sulphate. Total sulphate and organic mass concentrations decreased with leaner fuel spray nozzle conditions in the IP rig, though combustor AFR served as a better metric in the case of sulphate. Higher $\Delta P/P$ in the IP rig reduced EC, organic and sulphate mass concentrations.

Using the existing nvPM sampling system a considerable amount of chemical

speciation in the organic aerosol was possible, finding many chemical groups that are generally found in the PM phase in studies examining evolved plumes, without requiring the large exhaust plume evolution distances used in these studies, removing some of the uncertainty of background conditions and logistical restrictions of working within airports. In addition to researchers utilizing them, engine manufacturers routinely use these sampling systems. Rolls Royce will run the system on every engine emission test, averaging 3 tests per year; the systems will also run on their developmental combustion rigs, averaging 10 emissions tests per year. Different engine manufacturers make similar tests with systems that are built to the same design, making direct comparisons of this repeatable methodology possible. There is great opportunity to use these systems on real world systems for vPM measurement and potentially future regulation.

All observed chemical groups existed in what is described as the soot mode. One of the main limitations of the methodology applied here is that the organic nucleation mode material - which has been observed to dominate organic aerosol mass during idle engine conditions (Timko et al, 2010), - was not observed at near the engine exit distances of the two sources studied. This is not unexpected, as the nvPM reference system is designed to sample hot and dilute emissions purposely to suppress coagulation, which may have resulted in smaller nucleation mode particles being lost to diffusional and instrument losses.

The highly oxygenated low-volatility species found primarily during IP rig conditions could have future implications for combustor rig testing conducted by engine manufacturers. The application of quench air in combustor rig testing appears to

replicate chemical processes in the PM phase which have been observed to take place during artificial ageing of gaseous aircraft emissions in existing literature. Alongside this the existence of both oxygenated species at such close distances are important considerations for local air quality modelling, as these were emitted or formed rapidly. The most highly oxygenated factor observed here correlated with the mass of the lowest volatility OC by the OCEC Analyser, at temperatures greater than the nvPM threshold of 350 °C. This would be classed as nvPM under current nomenclature, however the mass analysers used to measure nvPM would not detect their contribution to its mass. Future studies should attempt to replicate this.

The AMS and PMF findings presented here show that the currently applied standardised nvPM sampling system can measure a range of organic vPM species which have been observed in aged plume studies. A comparison was made between similar ratios of alkanes to aromatics in the PM phase in the system presented here and those seen at greater distances in the literature. The highlighted consistencies of organic species between these two methodology types may indicate that a methodology similar to that which is applied here may serve as a cheaper yet effective alternative to study volatile particulates to aged plume measurements for engines of lower thrust. However, further work should include gas and particle sampling to unequivocally determine the potential use of such a sampling system for any future vPM standard.

Prior study has found no systematic statistically significant difference in chemical properties of particulate matter when comparing two downwind sampling distances (15m vs 30m and 30m vs 43m or 50m) on a given engine (Timko et al, 2010). Future investigations should examine the smallest distance from engines required in order to

acquire a representative sample for chemical speciation on engines of a given thrust. This would be crucial to inform any future regulation on vPM formed in aircraft exhaust.

5. Acknowledgments

The work contained in this paper was conducted during a PhD study supported by the Natural Environment Research Council (NERC) EAO Doctoral Training Partnership (Grant ref no NE/L002469/1) and Rolls-Royce plc whose support is gratefully acknowledged.

6. References

Anderson, B. E. et al. (1998) 'Airborne observations of aircraft aerosol emissions II: Factors controlling volatile particle production', Geophysical Research Letters, 25(10), pp. 1693–1696. doi: 10.1029/98GL00661.

Bauer, J. J. et al. (2009) 'Characterization of the sunset semi-continuous carbon aerosol analyzer', Journal of the Air and Waste Management Association, 59(7), pp. 826–833. doi: 10.3155/1047-3289.59.7.826.

Canonaco, F., Crippa, M., Slowik, J. G., Baltensperger, U., & Prévôt, A. S. H. (2013). SoFi, an IGOR-based interface for the efficient use of the generalized multilinear engine (ME-2) for the source apportionment: ME-2 application to aerosol mass spectrometer data. Atmospheric Measurement Techniques, 6(12), 3649–3661.

https://doi.org/10.5194/amt-6-3649-2013" https://doi.org/10.5194/amt-6-3649-2013

Crayford, A., Johnson, M., Llamedo, A., Williams, P. I., Madden, P., Marsh, R., and Bowen, P. SAMPLE III: Contribution to aircraft engine PM certification requirement and standard Third Specific Contract– Final Report, 2013. https://www.easa.europa.eu/document-library/research-projects/easa2010fc10-sc03.

EASA (European Aviation Safety Agency), 2009. Studying, sAmpling and Measuring of aircraft ParticuLate Emissions I (SAMPLE I). https://www.easa.europa.eu/document-library/research-reports/easa2008op13

Elsasser, M., Busch, C., Orasche, J., Schön, C., Hartmann, H., Schnelle-Kreis, J. & Zimmerman, R. (2013) Dynamic changes of the aerosol composition and concentration during different burning phases of wood combustion, *Energy and Fuels*, 27(8), pp. 4959–4968. doi: 10.1021/ef400684f.

Fujiwara, H., Nakaya, S., Tsue, M. & Okai, K. (2020) 'Emissions from HEFA Fuelled Gas Turbine Combustors', in Gupta, A., De, A., Aggarwal, S.K., Kushari, A. & Runchal, A. (ed.) *Innovations in Sustainable Energy and Cleaner Environment*. Springer, pp. 357–385. doi: https://doi.org/10.1007/978-981-13-9012-8.He, R. W. et al. (2018) 'Pro-inflammatory responses to PM 0.25 from airport and urban traffic emissions', Science of the Total Environment, 640–641, pp. 997–1003. doi: 10.1016/j.scitotenv.2018.05.382.

Hudda, N., Gould, T., Hartin, K., Larson, T. V., & Fruin, S. A. (2014). Emissions from an international airport increase particle number concentrations 4-fold at 10 km

downwind. Environmental Science and Technology, 48(12), 6628–6635. https://doi.org/10.1021/es5001566

Hudda, N., & Fruin, S. A. (2016). International Airport Impacts to Air Quality: Size and Related Properties of Large Increases in Ultrafine Particle Number Concentrations. Environmental Science and Technology, 50(7), 3362–3370. https://doi.org/10.1021/acs.est.5b05313

Hudda, N., Simon, M. C., Zamore, W., Brugge, D., & Durant, J. L. (2016). Aviation Emissions Impact Ambient Ultrafine Particle Concentrations in the Greater Boston Area. Environmental Science and Technology, 50(16), 8514–8521. https://doi.org/10.1021/acs.est.6b01815

ICAO. (2017). Annex 16 to the convention on international Civil aviation: Environmental protection, volume II: Aircraft engine emissions, international Civil aviation organization (ICAO) (4th ed.) July 2017 https://store.icao.int/annex-16-environmental-protection-volume-2-aircraft-engine-emissions.html.

Jayne, J.T., Pöschl, U., Chen, Y., Dai, D., Molina, L. T. and Worsnop, D.R., Kolb, C.E. & Molina, M. J. (1997) 'Pressure and Temperature Dependence of the Gas-Phase Reaction of SO3 with H2O and the Heterogeneous Reaction of SO3 with H2O/H2SO4 Surfaces', *Journal of Physical Chemistry*, 101(51), pp. 10000–10011. doi: https://doi.org/10.1021/jp972549z.

Jimenez, J. L. et al. (2009) 'Evolution of organic aerosols in the atmosphere', Science, 326(5959), pp. 1525–1529. doi: 10.1126/science.1180353.

Jonsdottir, H. R. et al. (2019) ‘Non-volatile particle emissions from aircraft turbine engines at ground-idle induce oxidative stress in bronchial cells’, Communications Biology. Springer US, 2(1), pp. 1–11. doi: 10.1038/s42003-019-0332-7.

Karanasiou, A., Minguillón, M. C., Viana, M., Alastuey, A., Putaud, J.-P., Maenhaut, W., Panteliadis, P., Močnik, G., Favez, O., & Kuhlbusch, T. A. J. (2015). Thermal-optical analysis for the measurement of elemental carbon (EC) and organic carbon (OC) in ambient air a literature review. Atmospheric Measurement Techniques Discussions, 8(9), 9649–9712. https://doi.org/10.5194/amtd-8-9649-2015

Kiliç, D. et al. (2018) ‘Identification of secondary aerosol precursors emitted by an aircraft turbofan’, Atmospheric Chemistry and Physics, 18(10), pp. 7379–7391. doi: 10.5194/acp-18-7379-2018.

Liu, P. S. K. et al. (2007) ‘Transmission efficiency of an aerodynamic focusing lens system: Comparison of model calculations and laboratory measurements for the aerodyne aerosol mass spectrometer’, Aerosol Science and Technology, 41(8), pp. 721–733. doi: 10.1080/02786820701422278.

Lobo, P., Rye, L., Williams, P.I., Christie, S., Uryga-Bugasjka, I., Wilson, C.W., Hagen, D.E., Whitefield, P.D., Blakey, S., Coe, H., Raper, D. & Pourkashanian, M. (2012). Impact of Alternative Fuels on Emissions Characteristics of a Gas Turbine Engine. Part I: Gaseous and Particulate Matter Emissions. Environmental Science & Technology, 46(19), 10805-10811. DOI: 10.1021/es301898u

Lobo, P. et al. (2015) ‘Measurement of aircraft engine non-volatile PM emissions:

Results of the Aviation-Particle Regulatory Instrumentation Demonstration Experiment (A-PRIDE) 4 campaign', Aerosol Science and Technology, 49(7), pp. 472–484. doi: 10.1080/02786826.2015.1047012.

Lobo, P. et al. (2016) 'Demonstration of a Regulatory Method for Aircraft Engine Nonvolatile PM Emissions Measurements with Conventional and Isoparaffinic Kerosene fuels', Energy and Fuels, 30(9), pp. 7770–7777. doi: 10.1021/acs.energyfuels.6b01581.

Lobo, P. et al. (2020) 'Comparison of standardized sampling and measurement reference systems for aircraft engine non-volatile particulate matter emissions', Journal of Aerosol Science. Elsevier Ltd, 145(November 2019), p. 105557. doi: 10.1016/j.jaerosci.2020.105557.

Lukachko, S. P. et al. (2008) 'Engine Design and Operational Impacts on Particulate Matter Precursor Emissions', Journal of Engineering for Gas Turbines and Power, 130(2), p. 021505. doi: 10.1115/1.2795758.

Makida, M., Yamada, H., Kurosawa, Y., Yamamoto, T., Matsuura, K. & Hayashi, S. (2006). Preliminary Experimental Research to Develop A Combustor for Small Class Aircraft Engine Utilizing Primary Rich Combustion Approach. ASME Turbo Expo 2006: Power for Land, Sea and Air, 1–8.

McKinney, R. G., & Hoke, J. B. (2013). Aero Gas Turbine Combustion: Metrics, Constraints, and System Interactions. Gas Turbine Emissions, 3–23. https://doi.org/10.1017/CBO9781139015462.004

McLafferty, F.W. & Turecek, F. (1993). Interpretation Of Mass Spectra (Fourth Edition). Sausalito, California: University Science Books.

Moore, R. H., Shook, M., Beyersdorf, A., Corr, C., Herndon, S., Knighton, W.B., Miake-Lye, R., Thornhill, K.L., Winstead, E.L., Yu, Z., Ziemba, L.D. & Anderson, A.B. (2015) 'Influence of jet fuel composition on aircraft engine emissions: A synthesis of aerosol emissions data from the NASA APEX, AAFEX, and ACCESS missions', *Energy and Fuels*, 29(4), pp. 2591–2600. doi: 10.1021/ef502618w.

Ng, N. L., Canagaratna, M. R., Zhang, Q., Jimenez, J. L., Tian, J., Ulbrich, I. M., Kroll, J. H., Docherty, K. S., Chhabra, P. S., Bahreini, R., Murphy, S. M., Seinfeld, J. H., Hildebrandt, L., Donahue, N. M., Decarlo, P. F., Lanz, V. A., Prévôt, A. S. H., Dinar, E., Rudich, Y., & Worsnop, D. R. (2010). Organic aerosol components observed in Northern Hemispheric datasets from Aerosol Mass Spectrometry. Atmospheric Chemistry and Physics, 10(10), 4625–4641. https://doi.org/10.5194/acp-10-4625-2010

Nicolosi, E. M. G., Quincey, P., Font, A., & Fuller, G. W. (2018). Light attenuation versus evolved carbon (AVEC) – A new way to look at elemental and organic carbon analysis. Atmospheric Environment, 175(December 2017), 145–153. https://doi.org/10.1016/j.atmosenv.2017.12.011

NIST Mass Spectrometry Data Center, 1990, Decane, US Secretary of Commerce, viewed 4/7/2020 < https://webbook.nist.gov/cgi/cbook.cgi?ID=C124185&Mask=200#Mass-Spec >

Olfert, J. S., Dickau, M., Momenimovahed, A., Saffaripour, M., Thomson, K.,

Smallwood, G., Stettler, M. E. J., Boies, A., Sevcenco, Y., Crayford, A. & Johnson, M. (2017) 'Effective density and volatility of particles sampled from a helicopter gas turbine engine', Aerosol Science and Technology, 51(6), 704–714. doi: 10.1080/02786826.2017.1292346.

Onasch, T. B., Jayne, J. T., Mortimer, I. P., Worsnop, D. R., Anderson, B. E., Herndon, S., & Miake-Lye, R. C. (2009). Chemical Properties of Aircraft Engine Particulate Exhaust Emissions. Journal of Propulsion and Power, 25(5), 1121–1137. https://doi.org/10.2514/1.36371

Paatero, P., & Tapper, U. (1994). Positive matrix factorization: A non-negative factor model with optimal utilization of error estimates of data values. Environmetrics, 5(2), 111–126. https://doi.org/10.1002/env.3170050203

Paatero, P. (1999). The Multilinear Engine—A Table-Driven, Least Squares Program for Solving Multilinear Problems, Including the n-Way Parallel Factor Analysis Model. Journal of Computational and Graphical Statistics, 8(4), 854–888. https://doi.org/10.1080/10618600.1999.10474853

Paatero, P., & Hopke, P. K. (2009). Rotational tools for factor analytic models. Journal of Chemometrics, 23(2), 91–100. https://doi.org/10.1002/cem.1197

Petzold, A. et al. (2005) 'Particle emissions from aircraft engines - A survey of the European project PartEmis', Meteorologische Zeitschrift, 14(4), pp. 465–476. doi: 10.1127/0941-2948/2005/0054.

Petzold, A., Marsh, R., Johnson, M., Miller, M., Sevcenco, Y., Delhaye, D.,

Ibrahim, A., Williams, P., Bauer, H., Crayford, A., Bachalo, W. D., & Raper, D. (2011). Evaluation of methods for measuring particulate matter emissions from gas turbines. Environmental Science and Technology, 45(8), 3562–3568. https://doi.org/10.1021/es103969v

Rye, L. and Wilson, C. (2012) 'The influence of alternative fuel composition on gas turbine ignition performance', *Fuel*. Elsevier Ltd, 96, pp. 277–283. doi: 10.1016/j.fuel.2011.12.047.

SAE. (2018). Standard ARP6320: Procedure for the continuous sampling and measurement of non-volatile particulate matter emissions from aircraft turbine engines. Warrendale, PA: SAE International. https://doi.org/10.4271/ARP6320. SAE

Stettler, M. E. J., Eastham, S., & Barrett, S. R. H. (2011). Air quality and public health impacts of UK airports. Part I: Emissions. Atmospheric Environment, 45(31), 5415–5424. https://doi.org/10.1016/j.atmosenv.2011.07.012" https://doi.org/10.1016/j.atmosenv.2011.07.012

Subramanian, R., Khlystov, A. and Robinson, A. (2006) 'Effect of peak inert-mode temperature on elemental carbon measured using thermal-optical analysis', *Aerosol Science and Technology*, 40(10), pp. 763–780. doi: 10.1080/02786820600714403.

Timko, M. Knighton, W. B., Herndon, S. C., Wood, E. C., Onasch, T. B., Northway, M. J., Jayne, J. T., Canagaratna, M. R., & Lye, R. C. M. (2010). Gas turbine engine emissions—part ii: Chemical properties of particulate matter. Journal of Engineering for Gas Turbines and Power, 132(6), 1–15. https://doi.org/10.1115/1.4000132

Timko, M. T., Albo, S. E., Onasch, T. B., Fortner, E. C., Yu, Z., Miake-Lye, R. C., Canagaratna, M. R., Ng, N. L., & Worsnop, D. R. (2014). Composition and sources of the organic particle emissions from aircraft engines. Aerosol Science and Technology, 48(1), 61–73. https://doi.org/10.1080/02786826.2013.857758

Ulbrich, I. M., Canagaratna, M. R., Zhang, Q., Worsnop, D. R., & Jimenez, J. L. (2009). Interpretation of organic components from Positive Matrix Factorization of aerosol mass spectrometric data. Atmospheric Chemistry and Physics, 9(9), 2891–2918. https://doi.org/10.5194/acp-9-2891-2009

Valavanidis, A., Fiotakis, K. and Vlachogianni, T. (2008) 'Airborne particulate matter and human health: Toxicological assessment and importance of size and composition of particles for oxidative damage and carcinogenic mechanisms', *Journal of Environmental Science and Health - Part C Environmental Carcinogenesis and Ecotoxicology Reviews*, 26(4), pp. 339–362. doi: 10.1080/10590500802494538.

van Berlo, D. Hullmann, M. and Schins, R.P.F. (2012) 'Toxicology of Ambient Particulate Matter'. In: Luch, A. (ed.) *Molecular, Clinical and Environmental Toxicology. Volume 3: Environmental Toxicology. Springer*, pp. 165–217.Yim, S. H. L., Stettler, M. E. J. and Barrett, S. R. H. (2013) 'Air quality and public health impacts of UK airports. Part II: Impacts and policy assessment', Atmospheric Environment. Elsevier Ltd, 67, pp. 184–192. doi: 10.1016/j.atmosenv.2012.10.017.

Yu, Z., Liscinsky, D. S., Winstead, E. L., True, B. S., Timko, M. T., Bhargava, A., Herndon, S. C., Miake-Lye, R. C., & Anderson, B. E. (2010). Characterization of lubrication oil emissions from aircraft engines. Environmental Science and Technology,

44(24), 9530–9534. https://doi.org/10.1021/es102145z

Yu, Z., Herndon, S. C., Ziemba, L. D., Timko, M. T., Liscinsky, D. S., Anderson, B. E., & Miake-Lye, R. C. (2012). Identification of lubrication oil in the particulate matter emissions from engine exhaust of in-service commercial aircraft. Environmental Science and Technology, 46(17), 9630–9637. https://doi.org/10.1021/es301692t

Yu, Z. et al. (2019) 'Mode-specific, semi-volatile chemical composition of particulate matter emissions from a commercial gas turbine aircraft engine', Atmospheric Environment. Elsevier, 218(September), p. 116974. doi: 10.1016/j.atmosenv.2019.116974.

Zhang, J. K., Ji, D. S., Liu, Z. R., Hu, B., Wang, L. L., Huang, X. J., and Wang, Y. S.: New characteristics of submicron aerosols and factor analysis of combined organic and inorganic aerosol mass spectra during winter in Beijing, Atmos. Chem. Phys. Discuss., 15, 18537–18576, https://doi.org/10.5194/acpd-15-18537-2015, 2015.